CREATING PHOTOREALISTIC VIRTUAL MODEL WITH POLARIZATION BASED VISION SYSTEM

偏光特性を利用したビジョンシステムによるリアリスティックな仮想現実感モデルの自動生成

by

Toru Takahashi

高橋　徹

A Master Thesis

修士論文

Submitted to

the Graduate School of

the University of Tokyo

on February 5 2002

in Partial Fulfillment of the Requirements

for the Degree of Master of Science
in Information Science

Thesis Supervisor: Katsushi Ikeuchi　池内 克史
Professor of Information Science

ABSTRACT

There is a growing interest in virtual reality system such as computer games, digital archives, many kinds of simulators and so on. And there are many researches on creating the virtual model by observing the real objects. In this paper, we propose the method for estimating the parameters of a bidirectional reflectance distribution function (BRDF) and creating the photorealistic virtual model by using the light stripe range finder and polarization based image capture system. Under the fixed point light source, we capture the range and the color images of the object which is rotated on the rotary table. Observing the variation of intensity occurred by the object rotation, we can estimate the parameters of BRDF (such as Torrance-Sparrow). Reflected light is separated into specularity and lambertian by the polarized light source and polarization filter setted in front of the camera, and that makes easy to estimate the parameters of BRDF. Estimating the parameters for each point of the object surface, we can correctly reproduce the surface optical properties even if the object surface has divergent optical properties.

論文要旨

近年、コンピューターゲームやデジタルアーカイブ、各種シミュレーターなどのバーチャルリアリティシステムに対する関心が非常に高くなってきている。それにともない、現実物体を観測することにより、仮想現実感システム用のモデルを自動生成する研究がさかんに行われている。本研究ではライトストライプレンジファインダーを利用して得られた形状モデルと、偏光を用いた画像撮影システムから得られたデータに基づき、BRDF のパラメーターを推定し、それにより仮想モデルを生成する手法について提案する。位置を固定した点光源下で、対象物体を回転台に乗せ各方面から画像とレンジデータの撮影を行う。光の入射角および反射角の変化にともなう物体表面上の輝度の変化から BRDF（Torrance-Sparrow モデル）のパラメーターを推定する。偏光光源とカメラの前にセットされた偏光板により、物体の反射光を表面反射と内部反射に分離し、それにより BRDF のパラメータ推定をより容易に行うことができる。物体表面上の各点ごとにパラメータ推定していくことにより、物体表面にさまざまな反射特性を持つ面が存在しても正しく表面の光学的特性を再現できる。

Acknowledgements

The author thanks the members of the Ikeuchi laboratory, especially the members of photometry group, for advising, helping my experimentation, and offering various software and hardware to be used in this work.

Contents

Chapter 1

Introduction

1.1 Background

It becomes more and more important to develop the easy method for getting the accurate reflectance information as the interest in virtual reality is growing. Currently, virtual reality system is used in a wide variety of applications including electronic commerce, simulation-and-training, and virtual museum walk-throughs. In spite of these many needs for virtual reality models, most of the virtual reality systems utilize models that are manually created by programmers. If we can build a system that automatically create the models for virtual reality system, we can drastically decrease modeling costs for virtual reality systems.

1.2 Related works

1.2.1 Image Bassed Rendering and Model Based Rendering

One major approach to building the virtual object model is the one which reconstructs the input images taken by camera. In recent several years, many techniques have been proposed for interpolating between views by warping input images, using depth information or correspondences between multiple images. The general notion of generating new views from pre-acquired imagery is called image-based rendering. Apple's QuickTime VR is the basic one. Gorter et al.[19] proposed the method for capturing the complete appearance of the real objects and scenes, and

rendering the images of the objects from new view positions. Unlike the traditional shape capturing method which is used in computer vision, they didn't use the fine geometric representation. Instead, they used the 4D function called Lumigraph. The Lumigraph is the subset of the complete plenoptic function which represents the complete flow of light in all position in all directions. Levoy et al.[20] also proposed the subset of the plenoptic function called Light Field. They interpreted the input images as two slices of 4D function. This function can completely characterizes the flow of light through unobstructed space in a static scene with fixed illumination.

Nishino et al. [26] proposed the another approach for image-based rendering. They used a fine geometric model and the eigen-texture which was texture-patchs made of pictures taken from various point of view and was reduced its data set by princial-component analysis. Wood et al.[21] also proposed the method which used a fine geometric model and point-based color information called Lumisphere. Lumisphere also reduced infromation quantity with the use of princial-component analysis.

The other approach to the problem is the one called model-based rendering. Usually, model-based rendering uses information of a fine geometry and a physical surface property. Sato et al.[14] built a virtual model of a coffee cup which was made of a fine geometric model and reflectance parameters used in a paticular reflectance model. They fixed the position of the camera and point light source and, then, putted the real object on the rotary table.

1.2.2 Separation of Reflection Components

When we make a virtual model with correct reflectance properties by observing real objects, we need to consider two reflection components: the specular reflection component and the diffuse reflection component. If we only map the observed image onto the object shape model as observed surface texture, we cannot reproduce the appearance of the object under different viewing and illumination conditions correctly. When highlights are observed in the original images, those highlights are

fixed on a certain position of the object surface permanently regardless of illumination and viewing conditions. Therefore, in order to model the reflection properties correctly, we have to separate the specular reflection and diffuse reflection.

In the computer vision research, several techniques to separate the reflection components have been developed. One major approach to the problem is the one that uses color as a clue. Most of color based methods are based on the dichromatic reflection model proposed by Shafer [10]. The dichromatic reflection model suggests that reflected lights from dielectric material have different spectral distributions between the specular and the diffuse reflection components. The specular component has a similar spectral distribution to that of the illumination. On the other hand, the diffuse component has an altered distribution by the colorants in the surface medium. Consequently, the color of an image point can be viewed as the sum of of two vectors with different directions in color space. Klinker et al.[11] observed that color histogram of a uniformly colored object surface makes the shape of *skewed* T with two limbs in the color space. One limb represents the purely diffuse points while the other represents highlight regions. Based on this observation, Klinker et al.[11] proposed an algorithm for automatically identifying the two limbs and using them to separate the diffuse and specular reflection components at each surface point. Sato and Ikeuchi [2] used a sequence of color images taken under actively varying light direction, and successfully separated the reflection components for each object surface point even if object surface is not uniformly colored.
Nayer et al. [6] used not only color but also polarization to separate the reflection components. Their proposed algorithm used the partial polarization included in the reflection in order to determine the color of specular component independently for each image point. The specular color imposes constraints on the color of the diffuse component, and the neighboring diffuse colors that satisfy these constraints are used to estimate the diffuse color vector for each image point.
All of these separation methods based on the dichromatic reflection model suffer from the common weakness in that they cannot work if the specular and diffuse reflection vectors have same direction in a color space. In this paper, we propose a new method for separating the reflection components using polarization. Unlike the

previously proposed methods, our method does not require that the diffuse color and the specular color are different. In order to separate the reflection components in a robust manner, we use a controlled illumination which is linearly polarized, and we take the images of an object through a polarization filter. Our method is able to separate the diffuse and specular reflection components for each image pixel independently, and therefore, it can be applied to objects with complicated surface textures.

1.3 Thesis Outline

In the second chapter, the representative reflection models are described, and, especially, Torrance-Sparrow reflectance model which is used in this paper is described in detail. In the third chapter, polarization mechanism which is used to separate the reflection components is explained. In the fourth chapter, data acquisition system, which contains the CCD camera, the light stripe range sensor, polarization filter, point light source, and rotary table, is described. In the fifth chapter, the details of the algorithm is described and the separation result is examined. In the sixth chapter, the parameters of the Toraace-Sparrow are estimated, and the result is presented. In the seventh chapter, by the estimated parameters, I synthesize the virtual images.

Chapter 2

Reflection Mechanism

A number of reflectance models have been proposed in the past by the researchers in the fields of applied physics and computer vision. In general, these models are classified into two categories: a diffuse reflectance model and a specular reflectance model.

2.1 Diffuse Reflection

A diffuse reflectance model represents reflected rays resulted from internal scattering inside surface medium.
When light strikes an interface between two different media, some percentage of the light passes through the boundary and the remaining portion of light is refleced. The penetrating light hits internal pigments of the objects, and is re-emitted randomly(Figure.2.1). This re-emitted light is called diffuse reflection, and Lambert is the first who modeled this phenomenon. The formula Lambert deduced is:

$$\begin{aligned} I_{diff} &= C_{diff}\vec{N}\cdot\vec{S} \\ &= C_{diff}\cos\theta_i \end{aligned} \tag{2.1}$$

where I_{diff}, C_{diff}, $\vec{N}$, $\vec{S}$, θ_i are the brightness, a propotional constant, the surface orientation,the light source direction, the angle between the light source direction and the surface orientation, respectively. The diffuse component does not depend on the angle of reflection but depend on the incident light.

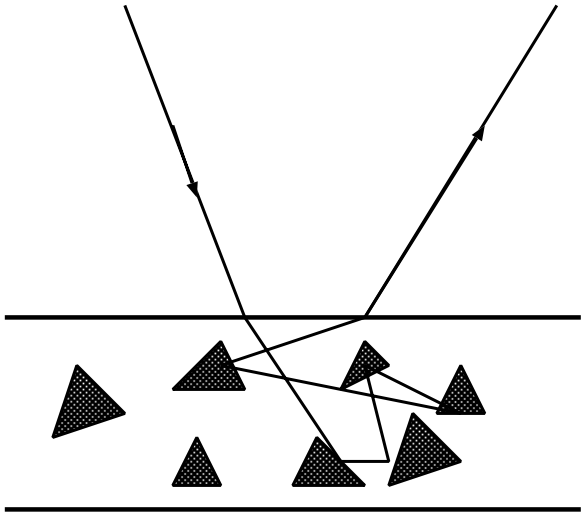

Figure 2.1: Diffuse reflection resulting from the internal scattering mechanism

2.2 Specular Reflection

A specular reflectance model, on the other hand, represents light rays reflected on the surface of the object. The surface may be assumed to be composed of microscopic planar elements, each of which has its own surface orientation diffent from the macroscopic local orientation of the surface. The result is the specular reflection component that spreads around the specular direction and that depends on the surface roughness for the width of the distribution.

Specular reflectance model can be derived from the two completely different approaches: physical optics based and geometrical optics based. The physical optics based approach uses electromagnetic theory and Maxwell's equations to study the propagation of light. On the other hand, geometrical optics based approach uses assumption of the short wave length of light and treats the propagation of light geometrically. The representative physical optics based model is the Beckman-Spizzichino model, and the representative geometrical optics based model is the Torrance-Sparrow model.

2.2.1 Physical optics based model

The physical models are directly derived from electromagnetic wave theory by usig Maxwell's equations. Beckmann and Spizzichino deduced their reflectance model by solving the Maxwell's equations by using Helmholts integral with Kirchoff's assumption on a perfect conductor surface. They made some assumptions to make up their reflectance model, as follows:

- The surface hight is assumed to be normally distributed.
- The radius of curvature of surface irregularities is large compared to the wavelength of incident light (Kirchoff's assumption).
- The surface is assumed to be a perfect conductor.
- The shadowing and masking of surface points by adjacent surface points are ignored.
- The light is assumed to be reflected only once and not to bounce between surface facets before scattered in the direction of the observer.
- The incident wave is assumed to be perpendicularly polarized.
- The incident wave is assumed to be a plane wave. This assumption is reasonable when the light source is at a great distance from the surface relative to the physical dimensions of the surface.

The Beckmann-Spizzino model consists of the specular lobe and specular spike components. The specular spike component is represented as a delta function and causes very sharp reflection when reflection angle equals to the incidence angle(specular angle). The specular lobe component is represented as a Gussian function and causes widely spreadding reflection.

2.2.2 Geometrical optics based model

The geometrical models are derived from simplifying many of the light propagation problems. Torrance and Sparrow obtained their reflectance model by assuming as follows:

- The surface is modeled as a collection of planer microfacets, and the facet slopes are assumed to be normally distributed.
- The size of palnner facets is much greater than the wave length of inciednt light. Therefore, it can be assumed that incident light rays are reflected by each facet in its specular direction only.
- Each facet is one side of a symmetric V-groove cavity.
- The light source is assumed to be at a great disatance from the surface so that all incident rays are regarded to be parallel to one another.

The Torrance-Sparrow model is represented by a Gaussian function of the surface roughness parameters.

2.3 General Reflectance Model

The Torrance-Sparrow model is aimed for modeling rough surface of any materials. The Beckmann-Spizzichino model describes the reflection from rough to smooth surface. The Torrance-Sparrow model is good approximation of the Beckmann-Spizzichino model when it is applied to the rough surface. So, physical optics based model is more general than the geometrical optics based. But, physical optics based model has very complex mathematical forms and is difficult to manipulate. Geometrical optics based model, however, has very simple function form, but it can not be applied to the smooth surface materials.
In order to combine the reflection models for the smooth surface and the rough surface, Nayer, Ikeuchi, and Kanade[12] proposed the general reflectance model. This model consits of three components: specular spike, specular lobe, and diffuse. Each of these components is represented by, respectively, these threee functions: the delta function, the Gaussian function, and the Lambertian's cosine function.
Let's assume that the surface is located at the origin of the coodinate frame, and that surface normal vector is in the direction of the Z axis. The beam illuminating the surface lies in the X-Z plane, and it's incident on the surafce is at an angle, θ_i. The observer is located at (θ_r, ϕ_r).

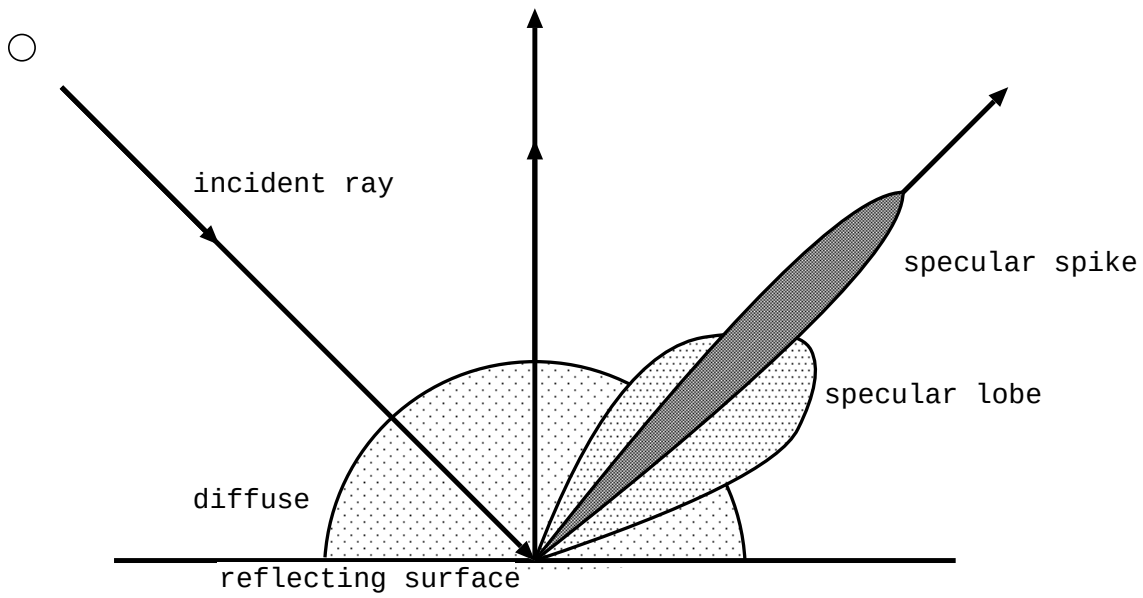

Figure 2.2: Diagram of the Unified Reflectance Model

Under this geometry, general reflectance model is represented as follows

$$I = C_{ss}\delta(\theta_i - \theta_r)(\phi_r) + C_{sl}\frac{\exp\left(-\alpha^2/2\sigma^2\right)}{\cos\theta_r} + C_{diff}\cos\theta_i \tag{2.2}$$

C_{ss}, C_{sl}, C_{diff} are constants which respectively represent the strength of the specular spike, specular lobe, and diffuse components. The α is the angle between the surface normal and the bisector of the viewing and light source directions. The σ is the parameter related to the Torrance-Sparrow surface roughness parameter.

The ratio C_{sl}/C_{ss} is dependent on the optical roughness of the surface. Mathematically, optical roughness is defined as

$$g = (2\pi\frac{\sigma_h}{\lambda}(\cos\theta_i + \cos\theta_r))^2 \tag{2.3}$$

where σ_h, λ are the root-mean-square of the height disrtribution, and the wavelength, respectively. For smooth surface ($g \ll 1$) , the spike component is dominant. As the roughness increases, however, the spike componet shrinks rapidly, and for rough surface $g \gg 1$, the lobe component begins to dominate. It is only for a

small range of roughness values that C_{sl} and C_{sb} are both significant. In this paper, the Torrance-Sparrow model is used for representing the diffuse and specular components.

$$I_m = I_{D,m} \cos\theta_i + I_{S,m} \frac{1}{\cos\theta_r} e^{-\alpha^2/2\sigma^2} m = R, G, B \tag{2.4}$$

where θ_i is the angle between the surface normal and the light source direction, θ_r is the angle between the surface normal and the viewing direction, α is the angle between the surface normal and the bisector of the light source direction and the viewing direction, $I_{D,m}$ and $I_{S,m}$ are the scaling factor for the diffuse and specular components, and σ is the standard deviation of a facet slope of the Torrance-Sparrow model.

In this model, the reflections bounced only once from the light source are considered. Therefore, this model is valid only for the convex objects. So, in this research, we use the objects for which inter-reflection does not affect our analysis significantly.

We refer to $I_{D,m}$ as the diffuse reflection parameters, and $I_{S,m}$ and σ as the specular reflection parameters.

Chapter 3

Polarization

3.1 Related works

Polarization has been used for several decades in the remote sensing research. Wolff and Boult [4] have proposed an algorithm which analyzes linear polarization states of highlights removal and material classification. Boult and Wolff [5] have also studied the classification of scene edges based on their polarization characteristics. Recently, Saito et al. [13] have proposed a method for measuring surface orientation of a transparent object using the degree of linear polarization in highlights observed on the object. Yoav et al. [7] have presented the method for classifying the transmitted image and the refelcted image on the transparent sheet.

3.2 Transmissivity of Polarization Filter

The method presented in this paper uses two linear polarization filters. One is placed in front of a point light source in order to polarize the light source linearly, and the other is placed in front of a camera to capture images through the linear polarization filter.

In this paper, we use the dichroic sheet polarizers as a polarization filter. We define the polarization filter's transmissivity T to the linearly polarized light as follows:

$$T = k_1 \cos^2\theta + k_2 \sin^2\theta \tag{3.1}$$

In the above equation, θ is the angle between the transmission axis of polarization filter and the vibrating surface of the incident light. If the polarization filter is ideal, k_1 equals to 1, and k_2 equals to 0. But real polarization filter has a little smaller k_1 than 1, and a little larger k_2 than 0.

In order to define the transmissivity to the non-polarized light, we introduce the transmissivity of a pair of the polarization filters(Figure.3.1). If we define θ as an angle between the transmission axises of closely attached two polarization filters, we get the transmissivity of a pair of the polarization filters.

$$T_{pair}(\theta) = k_1 k_2 \sin^2\theta + \frac{1}{2}(k_1^2 + k_2^2)\cos^2\theta \tag{3.2}$$

In the case of $\theta = 90^\circ$ and $\theta = 0^\circ$, we define a pair transmissivity of the polarization filters as follows:

$$H_{90} = T_{pair}(90^\circ) = k_1 k_2 \tag{3.3}$$

$$H_0 = T_{pair}(0^\circ) = \frac{1}{2}(k_1^2 + k_2^2) \tag{3.4}$$

We substitute the above equations to eq.(3.2), then we can simplify that equation as follows:

$$\begin{aligned} T_{pair} &= H_{90}\sin^2\theta + H_0\cos^2\theta & (3.5)\\ &= H_{90} + (H_0 - H_{90})\cos^2\theta & (3.6) \end{aligned}$$

H_{90} is called *closed transmissivity* or *extinction ratio*. And H_0 is called *open transmissivity*. Usually, open transmissivity has much larger value than closed transmissivty has, and so, the logarithm of the transmissivity(called *optical density*) is used to describe the polarization filter's property. The optical density is defined as follows:

$$\Delta_0 = \log\left(\frac{1}{H_0}\right) \tag{3.7}$$

$$\Delta_{90} = \log\left(\frac{1}{H_{90}}\right) \tag{3.8}$$

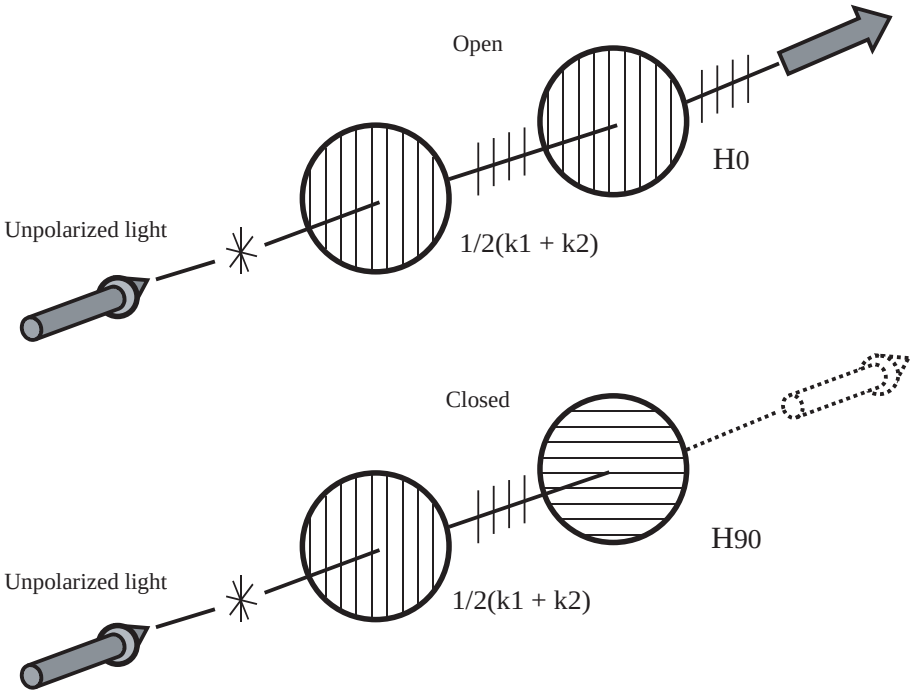

Figure 3.1: Transmissivity of a pair polarization filters

3.3 Separation of Reflection Componetns with Polarization

As described in the previous section, the image brightness value taken by sensor is described as:

$$I = I_d + I_s \tag{3.9}$$

where I_d represents the diffuse component and I_s represents the specular component.

When incident light is linearly polarized, the diffuse component tends to be unpolarized due to its internal scattering. In contrast, the specular reflection component tends to remain linearly polarized. Therefore, the observed brightness of the specular component can be expressed as a trigonometric function for polarization filter angle, and that of the diffuse component can be expressed as a constant. Thus the image brightness observed through a linear polarization filter is described as:

$$I = I_c + I_v(H_{90} + (H_0 - H_{90})\cos^2(\theta - \beta)) \tag{3.10}$$

where θ is the angle of the polarization filter and β is the phase angle determined by the projection of the surface normal onto the plane of the filter. H_{90} and H_0 are closed transmissivity and open transmissivity which are defined in the previous section.

It should be noted that in the above equation I_c is not equal to the real diffuse intensity, and I_v is not equal to the real specular intensity. The diffuse reflection component which is unpolarized is always attenuated by the polarization filter and the specular reflection component is also attenuated by the difference of the reflectivity between the light waves which are parallel or perpendicular to the incidence plane. [1]

The polarization state of reflected light dependents on several factors including the material of the reflecting surface element, and the type of reflection component, i.e. diffuse or specular. In order to describe the state of polarization of the reflected light, the Fresnel reflection coefficients $F_\perp(\eta, \psi)$ and $F_{||}(\eta, \psi)$ are used [4] (Figure.3.3). The Fresnel reflection coefficients determine the polarization of reflected

[1] The incidence plane includes the surface normal and the illumination direction.

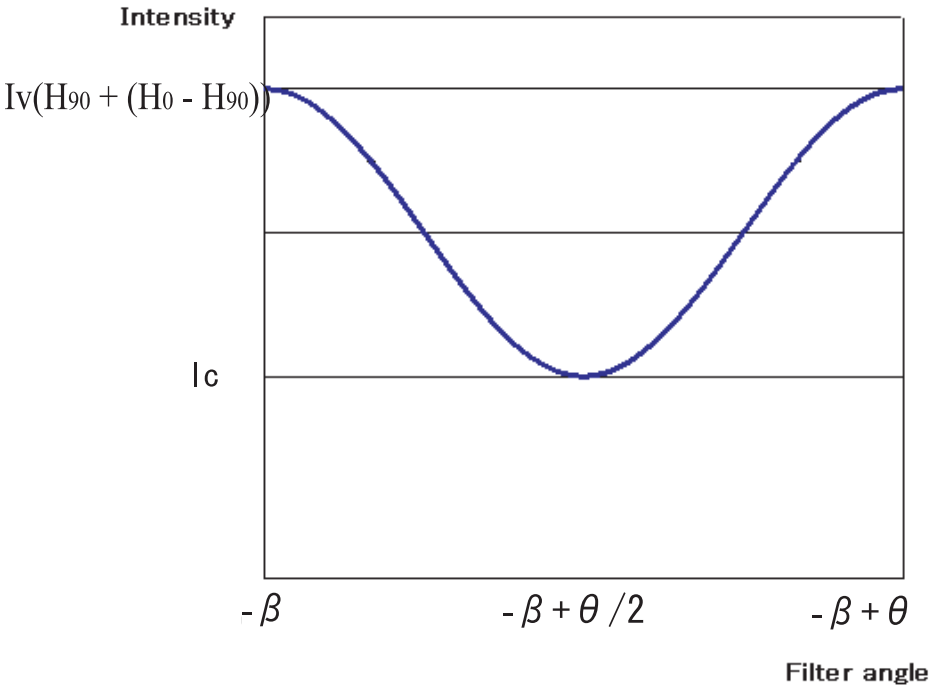

Figure 3.2: Relation between the imge brightness and the orientation of a polarization filter

light waves in the directions perpendicular and parallel to the plane of incidence, respectively, and determine the maximum and the minimum intensities which are observed when the angle θ of the polarization filter varies. The parameter η is the complex index of refraction of the surface medium and the parameter ψ is the incidence angle. Since we use a linearly polarized light source, we can assume that the intensity of the specular component observed through a linear polarization filter is guaranteed to become equal to zero at a certain angle. Hence, we obtain the following relation between I_v and specular reflection intensity:

$$q = \frac{F_{\perp}(\eta, \psi)}{F_{||}(\eta, \psi)} \tag{3.11}$$

$$I_v = \frac{q}{1+q} I_s \tag{3.12}$$

where I_s equals the specular reflection intensity.

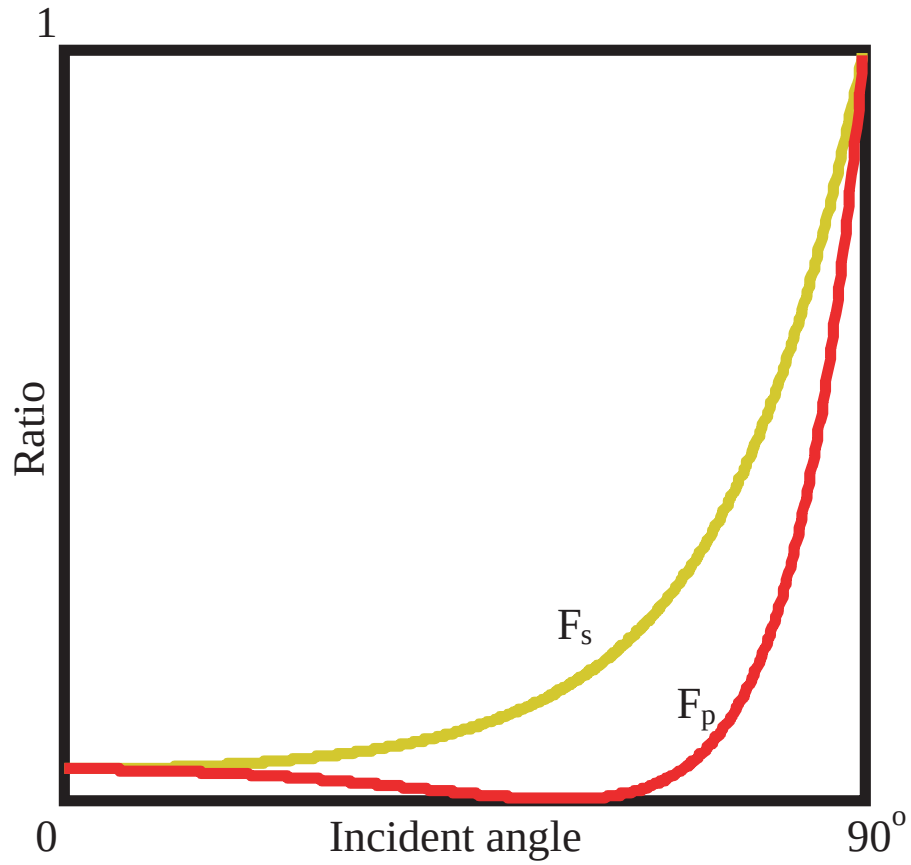

Figure 3.3: Relation between incident angle and Fresnel coefficients ($F_p = F_{||}$,$F_s = F_{\perp}$)

It is known that the diffuse component is also polarized when the viewing angle is close to 90 degrees, e.g., near the occluding contour of an object. However, the diffuse component becomes linearly polarized only in narrow region and the degree of polarization in the diffuse reflection component is generally negligible. Hence, we assume that the diffuse component is unpolarized in our analysis. The intensity of unpolarized light is attenuated by $1/2(k_1 + k_2)$ when it passes a linear polarization

filter. As a result, I_c and the diffuse component have a relation as below:

$$I_c = \frac{1}{2}(k_1 + k_2)I_d \tag{3.13}$$

where $\frac{1}{2}(k_1 + k_2)I_d$ is the observed intensity of the diffuse reflection.

Chapter 4

Data Acquisition System

4.1 Total Experimental Setup

The total experimental setup for the image acquisition system used in our experiment is illustrated in Figure 4.1. An object to be modeled in this experiment is placed on the rotary table. A sequence of range images and color images are captured as the object is rotated at a certain angle step. For each rotation step, one range image and thirty five color images, which are taken every five degrees polarization filter rotation in front of the CCD camera, are obtained.

4.2 Light Source

A xeon lamp is used as a light source. The lamp is small and placed far enough from the object so that we can assume the lamp is a point light source. In order to illuminate the object with linearly polarized light, a linear polarization filter is placed in front of the lamp.

4.3 Polarization Filter

In this experiments, dichromatic sheet polarizer is used as a polarization filter. The specification of the polarization filter which we use is as follows:

Coverage Wavelength Region $\cdots$ 350-650 nm

Transmissivity to non-polarized light beam $\cdots \frac{1}{2}(k_1 + k_2) = 32\%$

Open Transmissivity (H_0) $\cdots \geq 20\ \%$

Closed Transmissivity (H_{90}) $\cdots 10^{-4}$

4.4 CCD Camera

We use the Victor's KY-F70 3-CCD Digital Camera for image acquisition. The camera has 1360×1024 square pixels per CCD with progressive scanning and 3-CCD color accuracy.

4.5 Light Stripe Range Sensor

A range image is obtained using a light-stripe range sensor with a liquid crystal shutter and a color CCD video camera. Each range image pixel represents an (X, Y, Z) location of a corresponding point on an object surface. The same color camera is used for acquiring range images and color images. Therefore, pixels of the range images and the color images directly correspond. Color and range images are taken through a polarization filter.

The range sensor is calibrated to produce a 3×4 projection matrix Π which represents the translation between the world coordinate system and the image coordinate system. The location of the rotary table with respect to the world coordinate system is calibrated before image acquisition. Therefore, object location is uniquely determined by the translation matrix T.

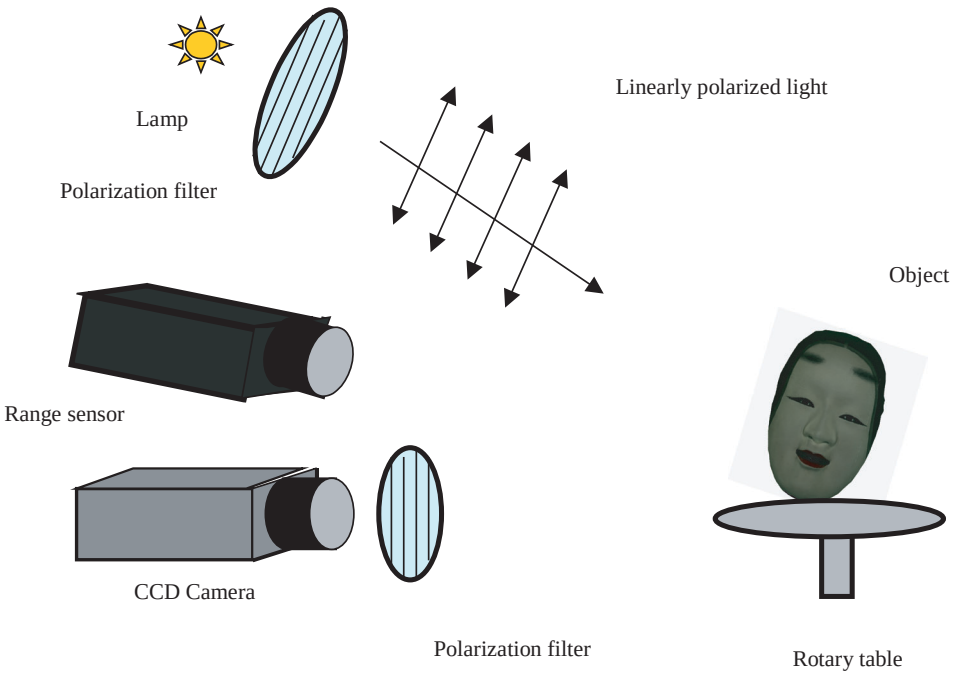

Figure 4.1: Image acquisition system

Chapter 5

Separation of Reflection Components

5.1 Separation Algorithm

In our experiments, images of a target object are taken every five degrees filer rotation, i.e., 35 images in total. Then, the maximum intensity I_{max} and the minimum intensity I_{min} are determined for every image pixel. Theoretically, only three images are sufficient for determining I_{max} and I_{min}. However, for increasing the robustness of estimation of I_{min} and I_{max}, we use more images by rotating the polarization filter. If $I_{min} - I_{max}$ for a certain pixel is less than a threshold, we consider the pixel to contain only the diffuse component. If $I_{max} - I_{min}$ is larger than a threshold value, we consider that the pixel contains the specular component and that $I_{max} - I_{min}$ is equal to $2I_v$ and I_{min} is equal to I_c.

In summary, our separation technique is proceeded as follows. First, a linear polarization filter is placed in front of the light source and camera. Second, input images of an object are captured for every 5 degree rotation of the polarization filter in front of the camera. Third, I_{max} and I_{min} are determined for each pixel. If $I_{max} - I_{min}$ is larger than a threshold value, we determine the pixel contains the specular component and the intensity of the specular component is obtained from $I_{max} - I_{min}$. I_{min} is used for determining the intensity of the diffuse component. Figure.5.1 shows the process of separating the reflection components.

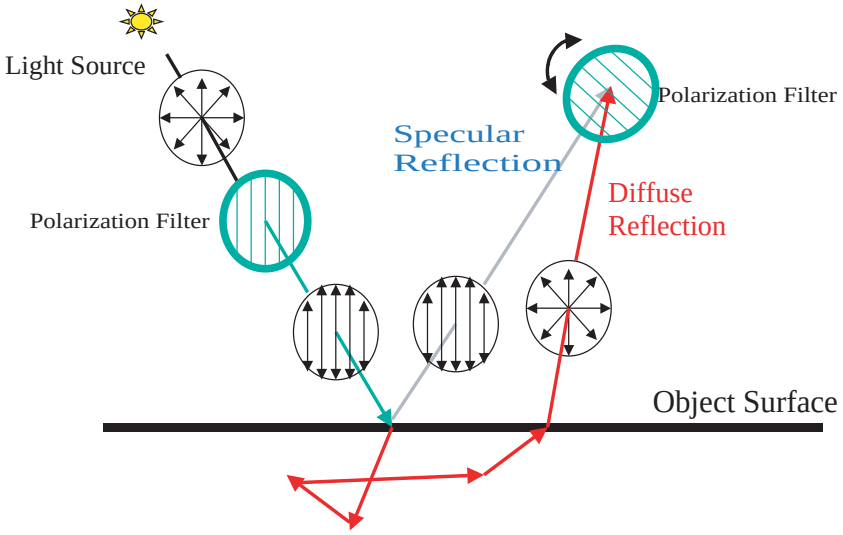

Figure 5.1: Mechanism of reflection componentns separation

5.2 Result

Figure.5.2 is one of the input images, and Figure.5.3 and Figure.5.4 show an corrensponding example of reflection component separation by using our proposed method. It shows that the specular and diffuse reflection components are successfully separated even if they have the similar color.

Figure.5.5 is another input image which has colorful texture. We use only polarization to separate reflection components, we are able to separate reflection components robustly. Figure.5.6 and Figure.5.7 are the results of reflection components separtion.

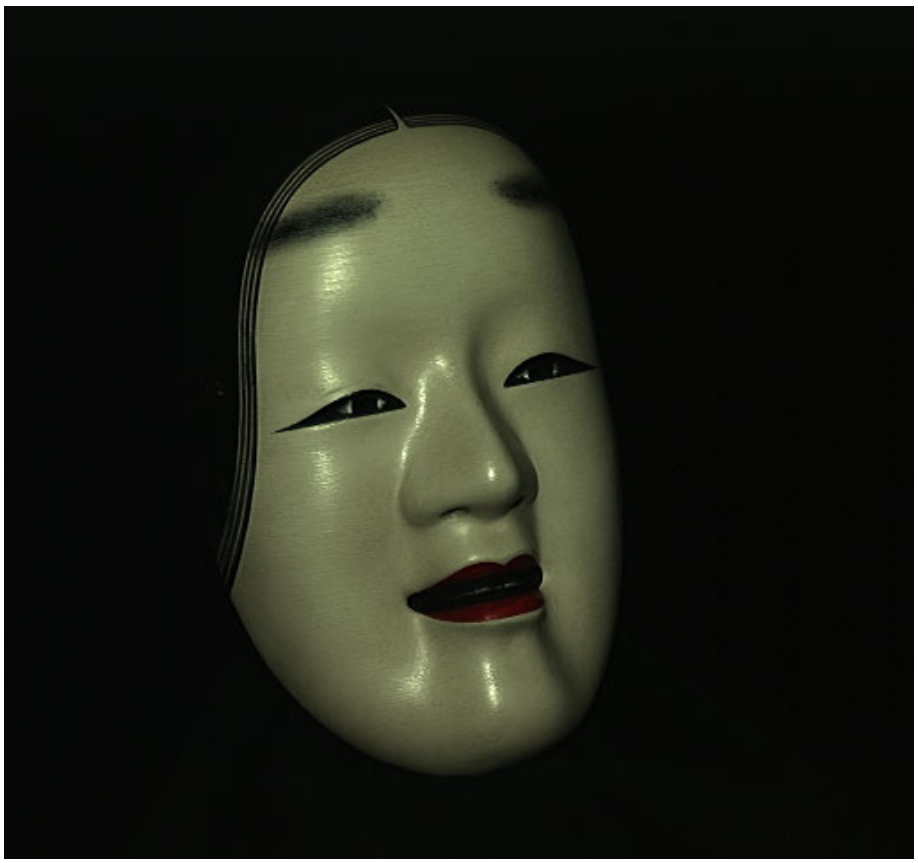

Figure 5.2: Input image taken without a polarization filter

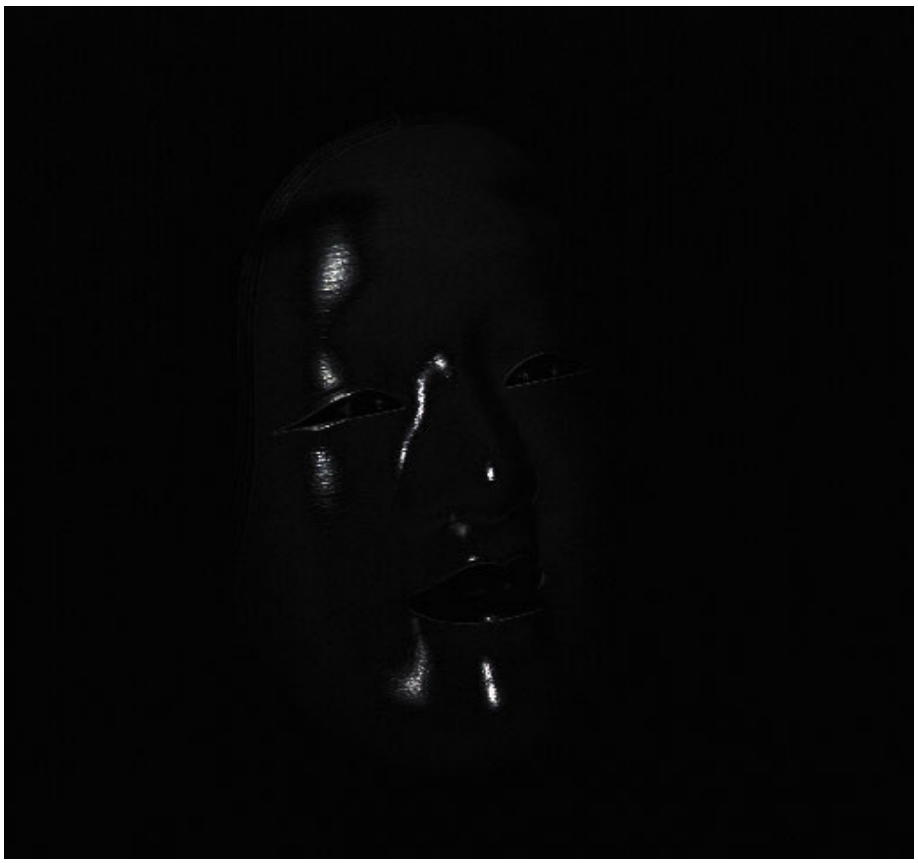

Figure 5.3: Separated specular component

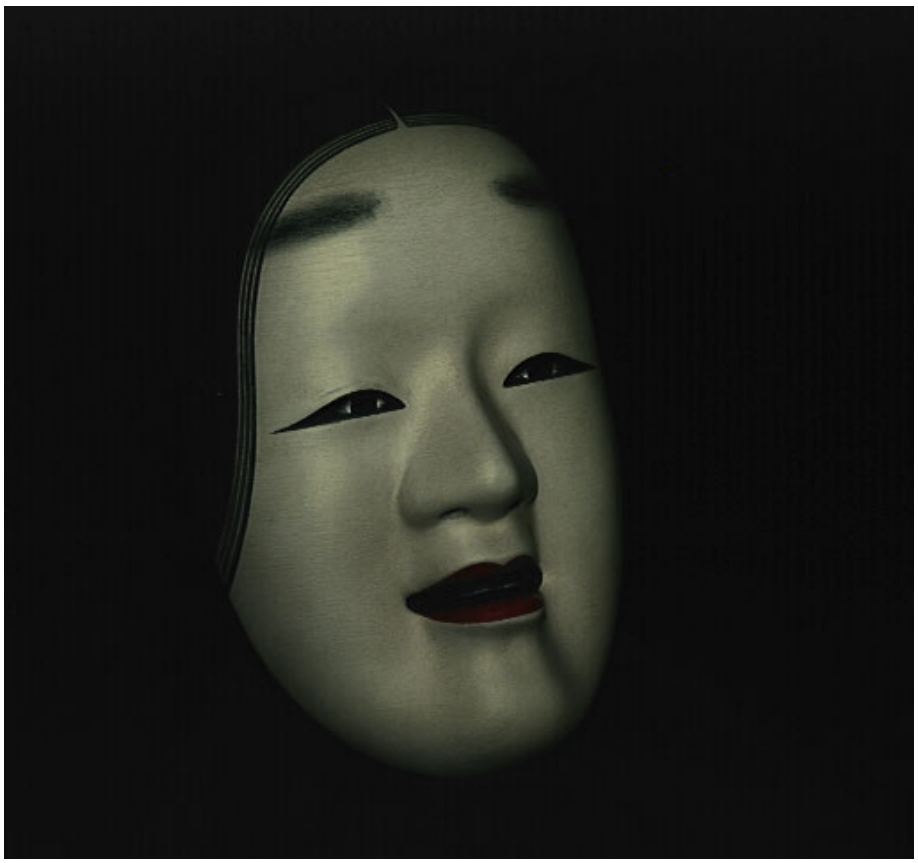

Figure 5.4: Separated diffuse component

Figure 5.5: Input image taken without a polarization filter

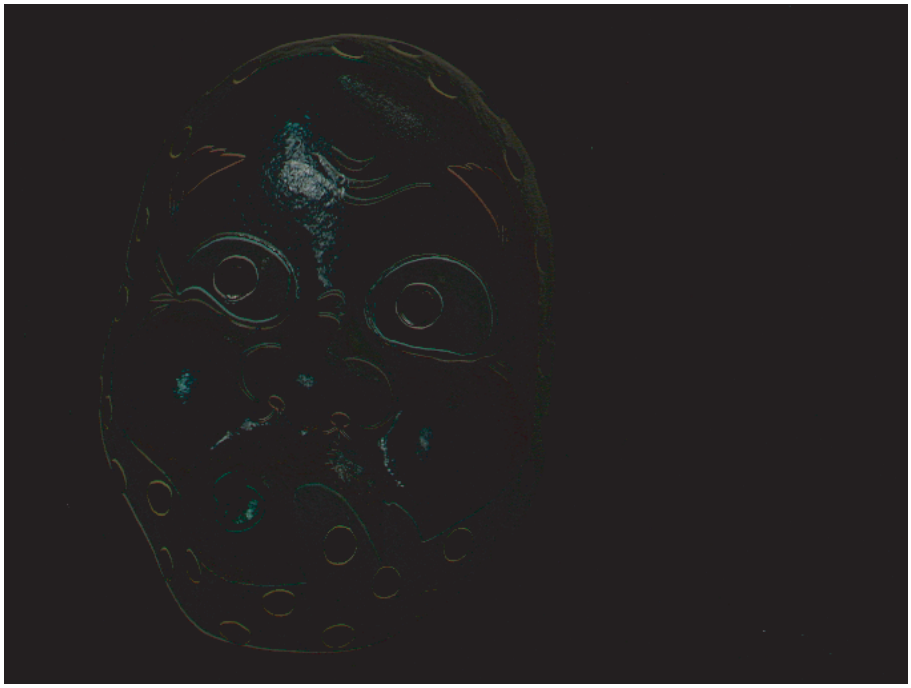

Figure 5.6: Separated specular component

Figure 5.7: Separated diffuse component

Chapter 6

Parameters Estimation

After separating the reflection components, we determine the reflectance parameters using the separated reflection component images.
In order to estimate reflectance parameters, we need not only reflection component images but also accurate geometric information. In the following sections, first, we explain the method for constructing object shape model by multiple range images. Second, we explain the detail of the diffuse parameters estimation. Last, we explain the algorithm for specular parameters estimation.

6.1 Surface Shape Modeling

A sequence of range images of the object is used to construct the object shape as a triangular mesh. Then, the number of triangles used for the object shape model is reduced by simplifying the object shape in order to compute the reflectance parameters efficiently.
One disadvantage of using the simplified object model is that a polygonal normal computed from the simplified triangular mesh model does not accurately approximate the real surface normal even if the object shape is preserved reasonably well. Thus, in order to estimate the reflectance parameters correctly, we compute the surface normals at every vertex of polygons by using the surrounding vertices.
In the following subsections, we describe reconstruction of a triangular mesh model of the object from a sequence of range images, and estimation of the fine surface

normals from surrounding vertices.

6.1.1 Shape modeling from range image merging

In order to reconstruct object shape as a triangular mesh model from multiple range images, following four steps are needed.

Alignment of all range images

All of the range images are measured in the coordinate fixed to the range sensor system, and so we need to align these images correctly. In order to align range images, we use the technique proposed by Nishino et al.[28].

Merging based on a volumetric representation

After all of the range images are aligned to a unique coordinate system, these range images are merged by the volumetric representation. In this experiment, we use the method proposed by Wheeler et al.[3].
First, we consider imaginary 3D volume grids around the aligned triangular patches. Next, in each voxel, we store the value, $f(x)$, of the signed distance from the center point of voxel, x, to the closet point of the object surface. The sign indicates whether the point is outside, $f(x) > 0$, or inside, $f(x) < 0$, the object surface, while $f(x) = 0$ indicates that x lies on the surface of the object.

Isosurface extraction from volumetric grid

The volumetric data is then used to construct the object surface which is represented as triangular mesh set. The marching cube algorithm [31] is used to construct a triangular mesh. The zero crossing of the implicit surface, $f(x) = 0$, is traversed in the volume grid.

Figure 6.1 shows the constructed object shape model which is made of triangular meshes.

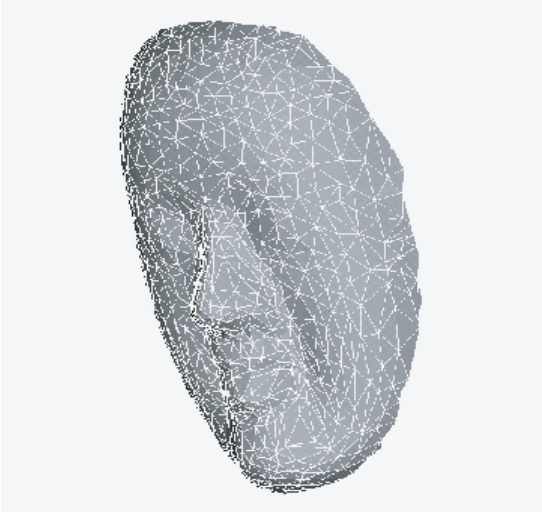

Figure 6.1: Constructed object shape model

6.1.2 Surface normal estimation

Polygonal normals computed from the triangular surface meshes are only approximation of the real object surface normals. If and only if the object surface is relatively smooth and does not have high curvature points, polygonal normals can approximate real surface well. In order to estimate reflectance parameters correctly at the every point of the object surface, we need three directions: the viewing direction, the light source direction, and the surface normal. And so, we have to compute surface normals more precisely.

For computing the accurate surface normals, we use the eigen vector of the covariance matrix of the neighboring 3D points. The covariance matrix of n 3D points $[X_l, Y_l, Z_l]$, whose centroid is $[\bar{X}, \bar{Y}, \bar{Z}]$, is described as follows:

$$C = \sum_{l=1}^{n} \begin{bmatrix} (X_l - \bar{X}) \\ (Y_l - \bar{Y}) \\ (Z_l - \bar{Z}) \end{bmatrix} \Big[(X_l - \bar{X}), (Y_l - \bar{Y}), (Z_l - \bar{Z}) \Big] \tag{6.1}$$

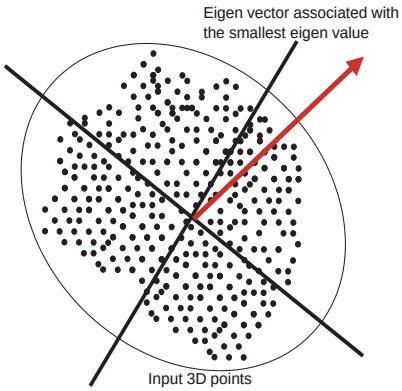

Figure 6.2: Principal component analysis for normal estimation

The eigen vector associated with the eigen value of the smallest magnitude can be considered the surface normal(Figure. 6.2). The surface normals are computed at all of the vertex points which consists triangular meshes. And surface normal within the triangular mesh is obtained by bilinear interpolation.

6.2 Diffuse Parameters estimation

Using the separated diffuse reflection image, we can estimate the diffuse reflection parameters $(I_{D,R}, I_{D,G}, I_{D,B})$ without undesirable effects from the specular reflection component. The incidence angle θ_i can be obtained by range sensor and camera calibration.
Figure 6.3 shows the estimated diffuse parameter image. We can see the object surface color which is not attenuated due to the incidence angle.

6.3 Specular Parameters estimation

After estimating the diffuse parameters, we also estimate the specular parameters $(I_{S,R}, I_{S,G}, I_{S,B}, \sigma)$ using the angle α and the angle θ_r as a known information.
As described in the Chapter 3, separated specular images are attenuated by a

certain ratio determined by Fresnel reflection coefficients. But attenuation ratio is constant overall highlight region, we can correctly estimate the specular parameters. More precisely, the Fresnel reflection coefficients are dependent on the incidence angle. However, the Fresnel coefficients are constant around the incidence angle less than 30 degree, and the specular reflection is observed only near the surface normal direction in our experimental setup. Therefore, by setting the light and camera in the same direction, we can assume that the Fresnel reflection coefficients are constant.

There is a significant difference between estimation of the diffuse and specular reflection. Diffuse reflection can be observed overall the object surface which is illuminated by a beam of light. On the other hand, specular reflection is observed from a limited viewing direction, and is observed over a narrow area of the object surface. So, we have to select the sampling pixels carefully for specular parameters estimation. We used the same strategy described in [14]. Figure 6.4 and 6.5 show the estimated σ and I_S which are projected on the mesh model.

Figure 6.3: Estimated diffuse parameter image

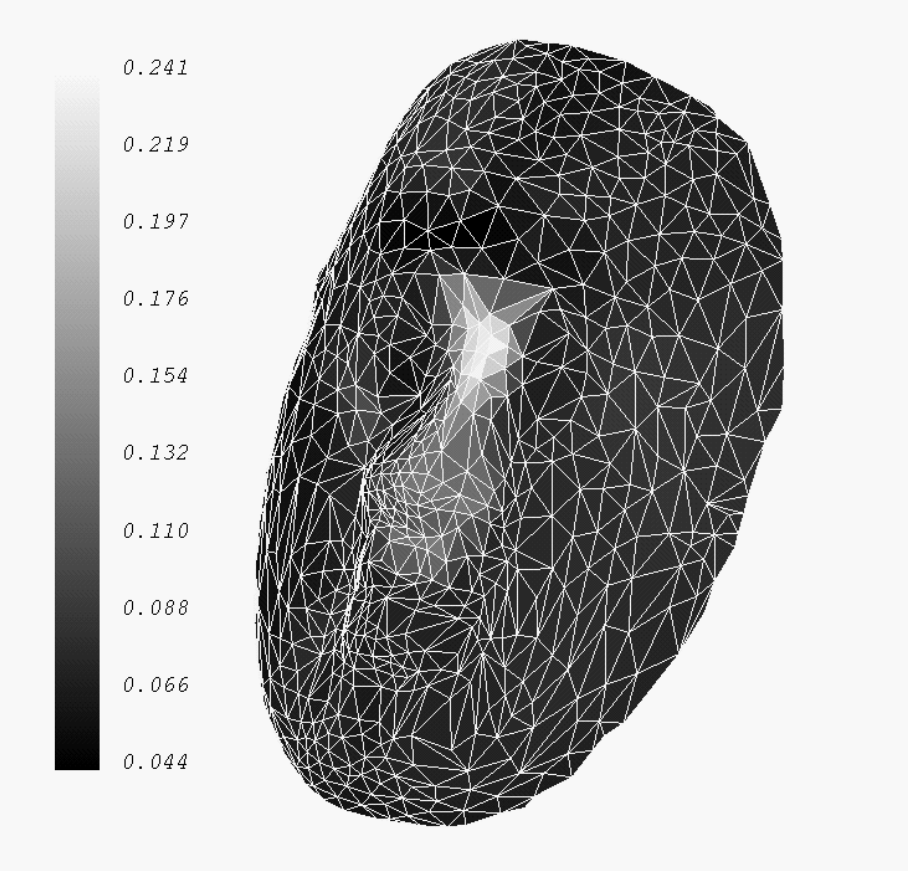

Figure 6.4: Specular parameter(σ) image

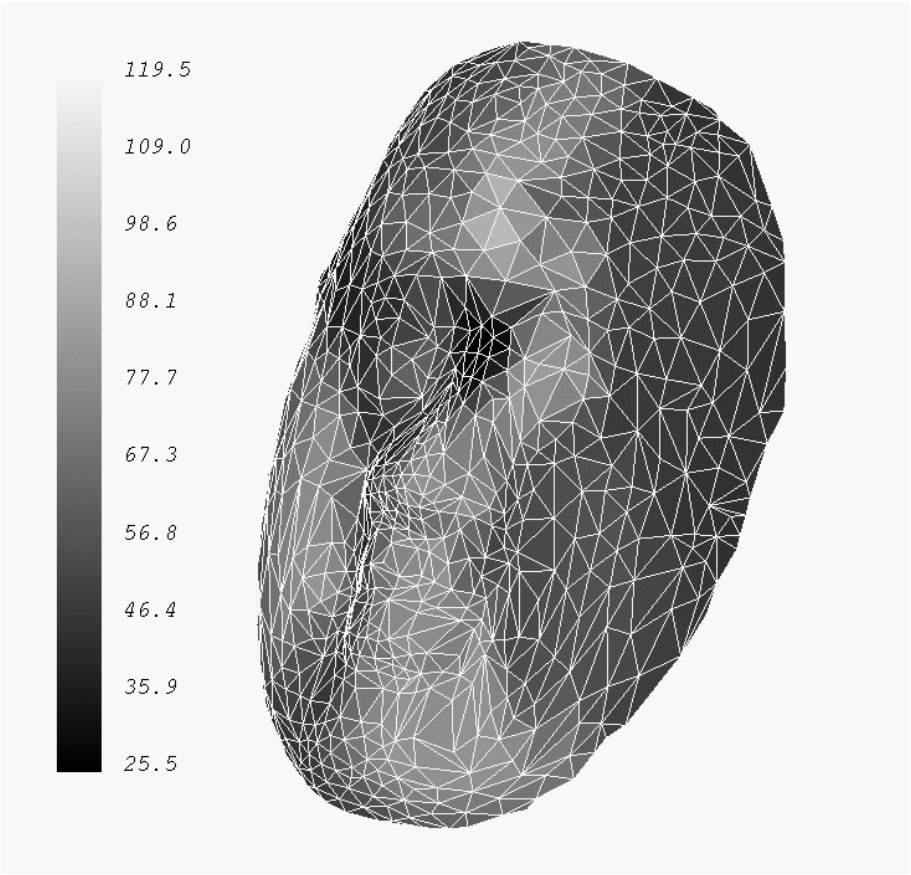

Figure 6.5: Specular parameter(I_S) image

Chapter 7

Synthesized Images

Using the diffuse and specular reflection parameters estimated in the previous section, and the surface mesh model of the object, we synthesized virtual images of the object under different illumination and viewing conditions. For synthesizing virtual images, the accurate surface normals obtained by the PCA are also used. Figure 7.1 shows the comparison between original images and synthesized images viewed from different directions.

Comparing the synthesized images with the original images, we notice that synthesized images are darker than the original images. This is, I think, caused by the variation of the polarizer's optical density with respect to the wavelength. Dichroic sheet polarizer has a different transmissivity to the different wavelength. In order to avoid this problem, we should have calibrated white balance every before capturing images without polarizer and before capturing images through polarizer.

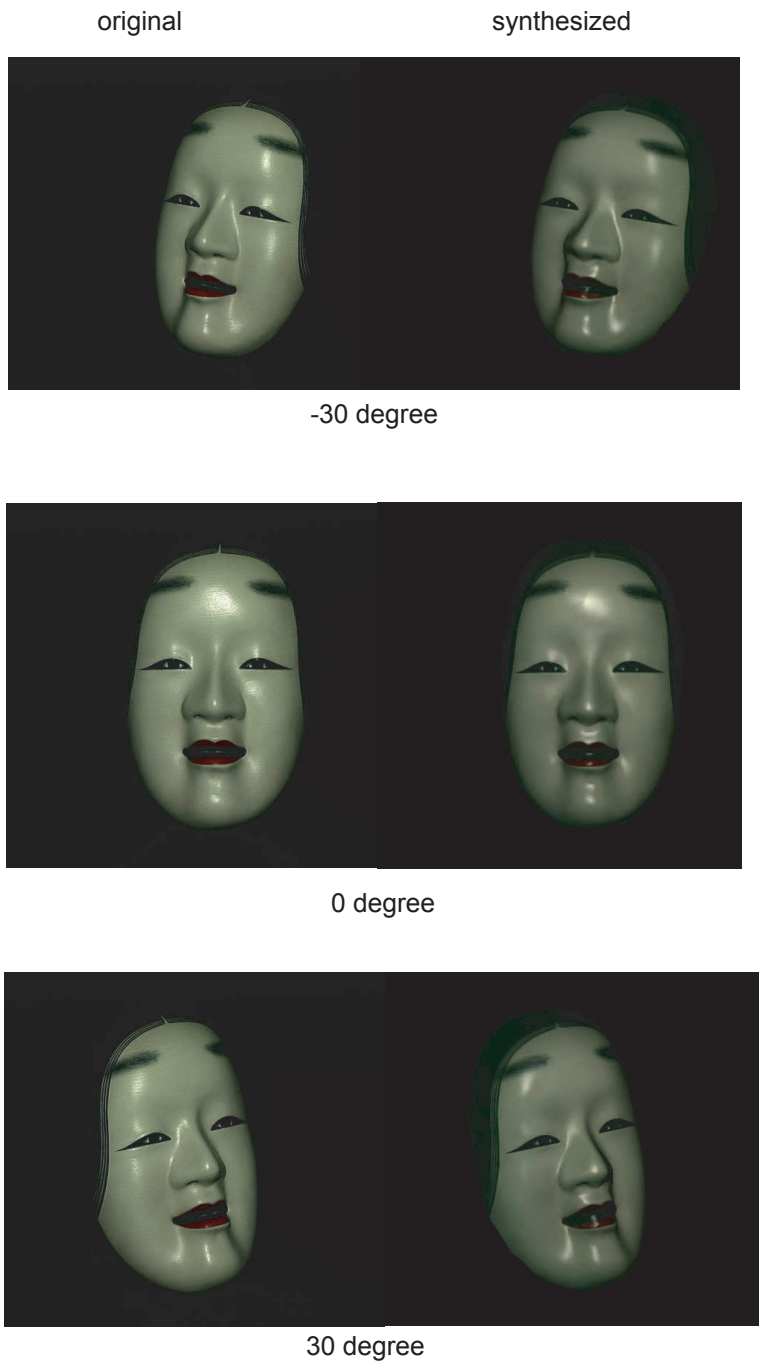

Figure 7.1: Comparison between input images and synthesized images

Chapter 8

Conclusion

In this paper, we proposed a new method for separating the reflection components using polarization. Unlike the previously proposed methods, our method does not require the difference of color between the specular reflection and diffuse reflection. So, our method can robustly separate the reflection components even if objects have a white texture and illumination color is white. After reflection components separation, we estimate the parameters of a reflection model by using the separated reflection components. By synthesizing virtual images under the arbitrary illumination and viewing, we have shown that the reflection parameters are successively estimated from the separated reflection components.

References

[1] K.Ikeuchi and K.Sato, "Determining reflectance properties of an object using range and brightness images," *IEEE Trans. on Pattern Analysis and Machine Intelligence*,vol.13, no. 11,pp.1139-1153,1991.

[2] Y.Sato and K.Ikeuchi, "Temporal-color space analysis of reflection," *Journal of Optical Society of America A*, vol.11, no.11,pp.2990-3002,November 1994.

[3] M.D.Wheeler,Y.Sato,and K. Ikeuchi, "Consensus surfaces for modeling 3D objects from multiple range images," *DARPAImage Understanding Workshop*, 1997.

[4] L.B.Wolff and T.E.Boult, "Constraining Object Features using a Polaization Reflectance Model," *IEEE Trans. on Pattern Analysis and Machine Intelligence*, Volo.13,No.7,pp.635-657, July 1991.

[5] T.E.Boult and L.B.Wolff, "Phisically based edge labeling," *Proceedings of Computer Vision and Pattern Recognition* ,pp.656-663,Maui,Hawaii,June 1991.

[6] S.K.Nayer,X.Fang, T.E.Boult, "Removal of specularities using color and polarization," *Proceedings of Computer Vision and Pattern Recognition '93*, pp.583-590, New York City, NY,June 1993.

[7] Y.Y.Schechner, J.Shamir and N.Kiryati, "Polarization-based Decorrelation of Transparent Layers: The Inclination Angle of an Invisible Surface," *Proceedings of International Conference on Computer Vision '99*,pp.814-819, 1999.

[8] S.K.Nayar and S.G.Narasimhan, "Vision in Bad Weather," *Proceedings of International Conference on Computer Vision*,1999.

[9] S.G.Narasimhan and S.K.Nayer, "Chromatic Framework for Vision in Bad Weather,"*Proceedings of Conference on Computer Vision and Pattern Recognition*,2000.

[10] S.Shafer, "Using color to separate reflection components," *Color Research and Applications*, Vol.10,pp.210-218,1985.

[11] G.J.Klinker, S.A.Shafer, and T.Kanade, "The measurement of highlights in color images," *International Journal of Computer Vision*, Vol.2,No.1,pp.7-32,1990.

[12] S.K.Nayer,K.Ikeuchi,T.Kanade,"Surface Reflection: Physical and Geometrical Perspecives,"*IEEE Trans. on Patter Analysis and Machine Intelligence*, Vol.13, No.7,pp.611-634,July 1991.

[13] M.Saito,Y.Sato,K.Ikeuchi,H.Kashiwagi, "Measurement of Surface Orientations of Transparent Objects Using Polarization in Highlight," *IEEE Trans.on Computer Vision and Pattern Recognition '99*, Vol.1,pp.381-386, Fort Collins,Colorado, June 1999.

[14] Y.Sato,M.D.Wheeler,K.Ikeuchi, "Object Shape and Reflectance Modeling from Observation," *Computer Graphics Proceedings,ACM SIGGRAPH'97*,pp. 379-387,Aug 1997.

[15] R.Ramamoorthi and Pat Hanrahan, "Analysis of Planer Light Fields From Homogeneous Convex Curved Surfaces Under Distant Illumination," *In SPIE Photonics West:Human Vision and Electronic Imaging VI*,2001.

[16] R.Ramamoorthi and Pat Hanrahan, "A Signal Framework for Inverse Rendering," *Computer Graphics Proceedings,ACM SIGGRAPH'01*, pp.117-128 ,2001.

[17] S.Tominaga and N.Tanaka, "Estimating Reflection Parameters from a Single Color Image," *IEEE Computer Graphics and Applications* ,Vol.22,No.5,pp.58-66,Sep./Oct.2000.

[18] M.Ashikhmin, S.Premoze and P.Shirley, "A Microfacet-based BRDF Generator," *Computer Graphics Proceedings,ACM SIGGRAPH'00*, pp.65-74,2000.

[19] S.J.Gorter,R.Grzeszczuk,R.Szeliski and M.F.Cohen, "The Lumigraph," *Computer Graphics Proceedings,ACM SIGGRAPH'96*, pp.43-54,Aug.1996.

[20] M.Levoy and P.Hanrahan, "Light Field Rendering," *Computer Graphics Proceedings,ACM SIGGRAPH'96*, pp.31-42,Aug.1996.

[21] D.N.Wood,D.I.Azuma,K.Aldinger,B.Curless,T.Duchamp,D.H.Salesin and W.Stuetzle, "Surface Light Fields for 3D Photography," *Computer Graphics Proceedings,ACM SIGGRAPH'00*,Aug.2000.

[22] P.Debevec,T.Hawkins,C.Tchou,H-P.Duiker and W.Sarokin. "Acquiring the Reflectance Field of a Human Face," *Computer Graphics Proceedings,ACM SIGGRAPH'00*,Aug.2000.

[23] T.Malzbender,D.Gelb and H.Wolters. "Polynomial Texture Maps," *Computer Graphics Proceedings,ACM SIGGRAPH'01*, Aug.2001.

[24] X.Liu,Y.Yu, and H.Shum. "Synthesizing Bidirectional Texture Functions for Real-World Surfaces," *omputer Graphics Proceedings,ACM SIGGRAPH'01*,Aug.2001.

[25] P.Debevec and J.Malik. "Recovering High Dynamic Range Radiance Maps from Photographs," *Computer Graphics Proceedings,ACM SIGGRAPH'97* ,Aug.1997.

[26] K.Nishino, Y.Sato and K.Ikeuchi, "Eigen-Texture Method: Appearance Compression and Synthesis based on a 3D Model," *IEEE Transactions on Pattern Analysis and Machine Intelligence*, Vol.23,No.11,pp.1257-1265, Nov.2001.

[27] K.Nishino, Z.Zhang and K.Ikeuchi, "Determining Reflectance Parameters and Illumination Distribution from a Sparse Set of Images for View-dependent Image Synthesis," *Proceedings of Eighth IEEE International Conference on Computer Vision'01*, Vol.1,pp.599-606,Jul.2001.

[28] K.Nishino and K.Ikeuchi, "Robust Simultaneous Registration of Multiple Range Images Comprising A Large Number of Points," *IPSJ CVIM*, Vol.2001,No.36,pp1-8,2001.

[29] R.Sagawa,K.Nishino,M.D.Wheeler and K.Ikeuchi, "Parallel Processing of Range Data Merging," *Proceedings of 2001 IEEE/RSJ International Conference on Intelligent Robots and Systems*, Vol.1,pp577-583,2001.

[30] R.Sagawa, K.Nishino and K.Ikeuchi, "Robust and Adaptive Integration of Multiple Range Images with Photometric Attributes," *Proceedings of IEEE Computer Vision and Pattern Recognition CVPR '01*, Vol.2,pp172-179,2001.

[31] W.E.Lorensen and H.E.Cline, "Marching cubes a high resolution 3D surface construction algorithms," *Computer Graphics (SIGGRAPH'87 Proceedings)*,vol.21,no.4, pp.163-169,1987.